Journal of Zhejiang University-SCIENCE A (Applied Physics & Engineering)
ISSN 1673-565X (Print); ISSN 1862-1775 (Online)
www.jzus.zju.edu.cn; www.springerlink.com
E-mail: jzus@zju.edu.cn

A uniform air flow distribution design strategy for use in tunnel transverse ventilation systems*

Ming-nian WANG[1,2], Tao DENG[1,2], Li YU[†‡1,2], Xu WANG[1,2]

[1]*School of Civil Engineering, Southwest Jiaotong University, Chengdu 610031, China*

[2]*MOE Key Laboratory of Transportation Tunnel Engineering, Southwest Jiaotong University, Chengdu 610031, China*

[†]E-mail: yuli_1026@swjtu.edu.cn

Received Apr. 9, 2018; Revision accepted Sept. 14, 2018; Crosschecked Dec. 6, 2018

Abstract: We focused mainly on a uniform air flow distribution design strategy for a multi-perforated air supply duct with a multi-blade opposed regulation damper. This design is especially required in tunnel transverse ventilation systems, in which a uniform air flow distribution is needed to dilute vehicle exhaust gases or vehicle emissions to acceptable concentrations. First, local resistance coefficients arising when air flows out of the duct through the damper were investigated by means of dimensional analysis and computational fluid dynamics (CFD) simulation, and a mutual authentication was performed with 3D and 2D simulation results. This revealed that the ratio of the velocity in the duct and the damper, and the blade opening angle are the two main factors affecting the resistance coefficient. Second, theoretical analysis based on Bernoulli's equation was implemented to establish the relationship between the local resistance coefficient and the pressure drop. Based on the simulation results, a uniform air flow distribution design strategy corresponding to the opening angle adjustment was obtained. Finally, a calculation case study was carried out, and sufficient consistency between the theoretical and numerical calculation results was achieved, verifying the reliability of the design strategy.

Key words: Multi-perforated duct; Computational fluid dynamics (CFD); Flow resistance; Uniform flow distribution; Transverse ventilation

https://doi.org/10.1631/jzus.A1800230 **CLC number:** U453.5

1 Introduction

Uniform air flow distribution is an important and fundamental issue for many types of equipment and is required especially in many engineering fields, such as in air conditioning systems (VanGilder and Schmidt, 2005), heat sinks for electronic devices in cooling systems (Kim et al., 1995), piping systems (Ascough and Kiker, 2002), chemical reactors (Kareeri et al., 2006), and nuclear reactors (Wang et al., 2001). In road tunnel engineering, uniform distribution of air throughout the length of the tunnel is especially needed to dilute vehicle exhaust gases or emissions to acceptable concentrations in a transverse ventilation system (we use this term in this study to include both transverse and semi-transverse ventilation systems). In a transverse ventilation system, a purpose-built air supply duct runs along the length of the tunnel, with discrete openings into the tunnel at intervals along its length, and each of these openings is fitted with a motorized damper (Lesser et al., 1987; Li and Chow, 2003). The purpose-built air supply duct is a kind of multi-perforated duct.

A multi-perforated air supply duct indicates an air flow channel with a closed end and equally spaced, uniformly sized side orifices installed on the surface of the channel. The area of each orifice is usually

‡ Corresponding author

* Project supported by the National Natural Science Foundation of China (No. 51308472) and the Sichuan Provincial Science and Technology Project of China (No. 2018JY0566)

ORCID: Li YU, https://orcid.org/0000-0002-8146-1583

quite small compared with the channel surface. Apart from tunnel engineering, multi-perforated ducts are widely used in a lot of other industries, such as medicine, chemistry, and agriculture. That is because they can play the role of a flow divider capable of ejecting flow through the orifices (El Moueddeb et al., 1997; Kareeri et al., 2006; Foust and Rockwell, 2007). Due to changes of pressure in the longitudinal direction (flow direction), the discharge angles and flow rates of the stream released from the orifices are known to differ at each location (El Moueddeb et al., 1997; Chen and Sparrow, 2009a; Singh and Rao, 2009). To achieve uniformity of air flow in a multi-perforated duct, i.e. a uniform flow rate among orifices, two strategies are often adopted. One is to ensure a constant static pressure in the whole air supply duct by appropriate adjustment of the cross section of the duct along the longitudinal direction. Ye (2017) developed a systematic design method to realize a uniform air flow distribution with this strategy. The other is to maintain a constant cross section along the duct and adopt a different opening ratio for the orifices at different locations. As for tunnel ventilation systems, considering the immense length of the air supply duct and the limited clearance area of the tunnel, the latter strategy is always selected. A lot of work has been done on the flow distribution and pressure characteristics of constant cross section multi-perforated ducts. Lee et al. (2012) investigated the influence of orifice configuration on exit flow characteristics. Chen and Sparrow (2009a) performed an analytical and experimental study of the characteristics of the flow rate distribution using multi-perforated tubes where rectangular orifices were installed. El Moueddeb et al. (1997) represented the flow rate distribution characteristics in multi-perforated tubes with orifices of various shapes as a 1D equation using the internal static pressure. Some investigations (Ibukiyama, 1957; Jo et al., 2017) focused on a systematic design method for realizing a uniform air flow distribution by regulating the opening ratio of orifices in tunnel air supply ducts with a constant cross section. However, all these studies considered only the orifice configuration (shape, pitch, and size). The structure of the orifice was rarely considered, especially for air supply ducts in tunnel engineering.

Multi-blade opposed regulation dampers are specifically engineered for gas turbine exhaust applications, in which precise flow control is required. Standard actuators include pneumatic, electric, hydraulic, and manual systems. This kind of damper can be directly installed on the air duct, and the outflow can be conveniently and flexibly adjusted by setting different blade opening angles. Thus, this damper can play an important role in a tunnel transverse ventilation system to achieve effective air flow control. In this study, we aimed to develop a uniform air flow distribution design strategy in a multi-perforated air supply duct with a multi-blade opposed regulation damper. Both the computational fluid dynamics (CFD) simulation method and theoretical analysis were implemented to investigate the air flow through a three-blade opposed regulation damper to determine the flow resistance coefficients corresponding to the opening angle. The results of this investigation will be helpful in the preliminary design of tunnel transverse ventilation systems.

2 Flow resistance through a multi-blade damper

2.1 Multi-blade opposed regulation damper

Multi-blade opposed regulation dampers are specifically engineered for gas exhaust applications, in which precise flow control is required. They can be installed directly on the air duct, and the air volume can be adjusted conveniently and flexibly by changing the opening angle of the blade. The most common actuators include electric and manual systems. The shape of the damper is shown in Fig. 1.

The height of the damper generally ranges from 0.22 m to 0.25 m, and a blade usually has a width of nearly 0.20 m. Under most circumstances, dampers are galvanized to be capable of working under quite high temperatures, which is of great significance for tunnel smoke exhaust in fire situations.

In a tunnel transverse ventilation system, the damper size chosen depends on the air volume requirement for unit length of the tunnel and the interval of dampers, because both the minimum and maximum velocities that flow out of each damper at its maximum opening ratio should be restricted. Under such conditions, dampers of a size close to or smaller than 0.6 m^2 are always adopted in transverse ventilation system designs (Ibukiyama, 1957). Therefore, in this study, a three-blade damper was taken as the analysis object to give the investigation on the best universality. The dimension parameters of the damper are listed in Table 1.

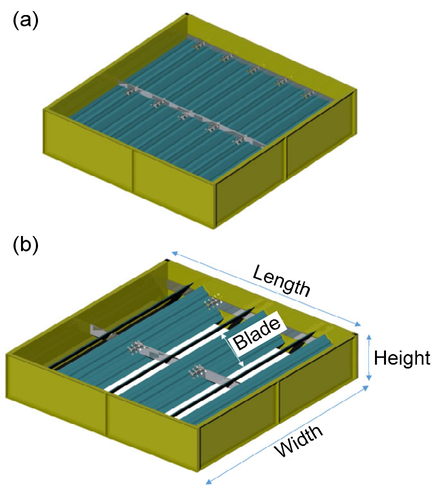

Fig. 1 Multi-blade opposed regulation damper
(a) Blades closed; (b) Blades open

Table 1 Dimension parameters for the investigated damper

Parameter	Value	Parameter	Value
Damper length (m)	0.60	Damper width (m)	1.00
Blade quantity	3	Blade width (m)	0.20
Damper height (m)	0.25		

2.2 Analysis of the air flow in the duct with the damper

A schematic diagram of an air supply duct with a three-blade damper is shown in Fig. 2. In the figure, θ is the opening angle of the blade, A and a are the areas of the duct and damper, respectively, and V and v are the air flow velocities of the duct and damper, respectively.

Applying Bernoulli's equation between a duct (section 1) and an outflow (section 2), a balanced equation can be obtained as

$$P_{\mathrm{r}}+\frac{\rho}{2}V^2=P_{\mathrm{e}}+\frac{\rho}{2}v^2+\xi\frac{\rho}{2}v^2+\Delta P_{\mathrm{f}}, \tag{1}$$

where P_{r} and P_{e} represent the static pressures of sections 1 and 2, respectively, ρ is the air density, ξ is the local resistance coefficient arising when air flows out of the duct through the damper under an opening angle of θ, and ΔP_{f} is the pressure drop caused by frictional resistance.

In this investigation, for simplicity and considering the short distance of the flow path, frictional resistance was not taken into account. A deformation of Eq. (1) leads to the expression for the local resistance coefficient ξ:

$$\xi=\frac{2\left(P_{\mathrm{r}}-P_{\mathrm{e}}\right)}{\rho v^2}+\left(\frac{V}{v}\right)^2-1. \tag{2}$$

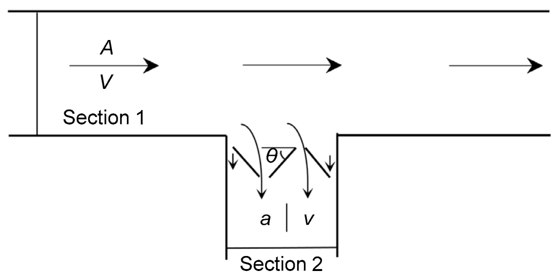

Fig. 2 A schematic representation of a duct with a damper

2.3 Flow resistance of the damper

The local resistance coefficient is a dimensionless quantity related to the shape of the local obstacles and the Reynolds number. At low Reynolds numbers, especially for a laminar flow, the local resistance coefficient can be greatly affected by the Reynolds number. However, when the Reynolds number is high, it has little effect on the local resistance coefficient (Yu, 2013). In this investigation, we focused mainly on viscous flow within a high Reynolds number, ranging from 1×10^5 to 5×10^6. Thus, we characterize ξ only as a function of the velocity ratio (v/V) and opening angle (θ):

$$\xi=f\left(\frac{v}{V},\theta\right). \tag{3}$$

CFD simulation with Fluent 15.0 was taken as the analysis method to determine how these two factors affect ξ. To make the simulation results more reliable, both 2D and 3D models were built (Fig. 3), to enable mutual authentication. Both models consist three parts: an air supply duct, a three-blade damper,

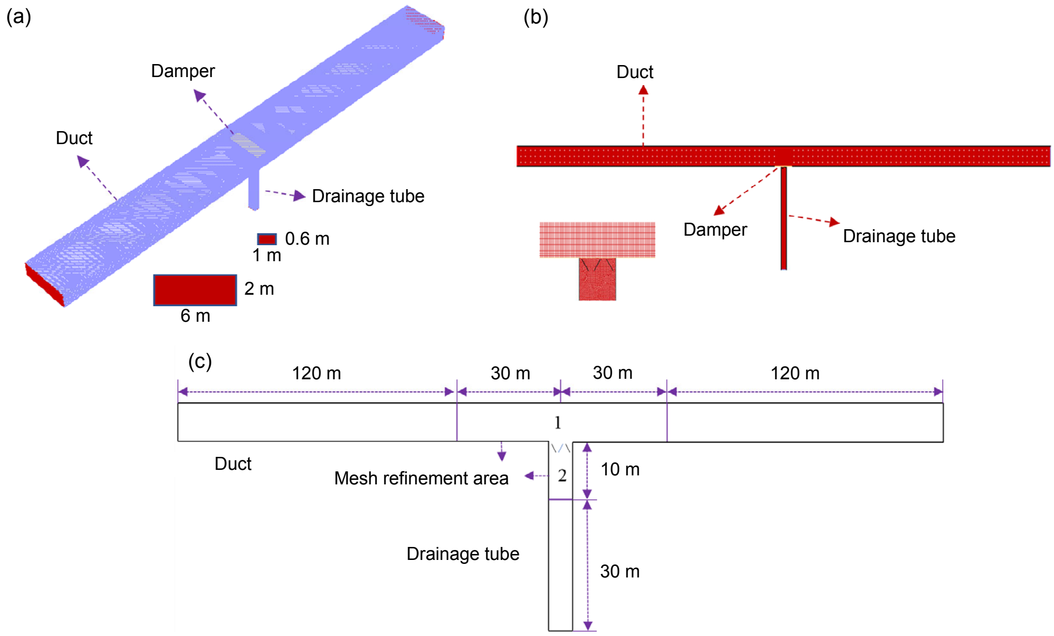

Fig. 3 Representation of CFD models and the mesh scheme
(a) 3D model; (b) 2D model; (c) Mesh refinement scheme

and a drainage tube. The drainage tube is used to monitor the static pressure in the outflow section. In the 3D model, the duct is 300-m long, 6-m wide, and 2-m high; the drainage tube is 60-m long, 1-m wide, and 0.6-m high. In the 2D model, the height of the duct was set as 1.5 m to match the hydraulic diameter with the 3D model. For both models, the lengths of the duct and drainage tube were set as 60 times the length of the corresponding hydraulic diameters to avoid the influence of flow entrance boundary conditions (Ji et al., 2010). The two models were implemented with the same mesh refinement scheme: the grids were refined within 30 m and 10 m of the damper in the duct and drainage tube, respectively.

Selecting an appropriate turbulence model is vital for numerical simulation of air flow through the damper by means of the CFD method. The k-ε turbulence model is known to be able to make relatively accurate calculations in the event of big changes in curvatures of streamlines, at the same time being suitable for rotation and the flow field of recirculation. So, it is natural to start with the original k-ε model because of its many successful applications (Chen and Sparrow, 2009b; Farajpourlar, 2017). There are three kinds of k-ε models: renormalized group real k-ε (RNG), realizable k-ε (REAL), and standard k-ε. In this study, we compared these three models and found that the REAL model provided the best convergence property. So, it was chosen for the numerical simulation.

To compare the 3D and 2D methods, four different velocity ratios (0.2, 0.3, 1.0, and 1.5) were simulated. The opening angle θ was fixed at 60° and the entrance velocity was 8 m/s for each simulation. The velocity vector distribution fields for the different velocity ratios are shown in Fig. 4. Using Eq. (2), local resistance coefficients of the series of simulations were calculated (Fig. 5).

According to Figs. 4 and 5, simulation results from the 2D and 3D methods fit well, showing that both methods are feasible to determine the resistance coefficients. Based on these results, the air flow in the duct with the multi-blade damper under velocity ratios ranging from 0.1 to 16.7 and opening angles ranging from 22.5° to 90° was simulated with the 2D method. The local resistance coefficients were calculated (Table 2).

Following the analysis of the data in Table 2, the following conclusions were drawn:

1. When the opening angle θ is constant, the local resistance coefficient ξ tends to increase as the velocity ratio v/V decreases. This is especially obvious when v/V is small.

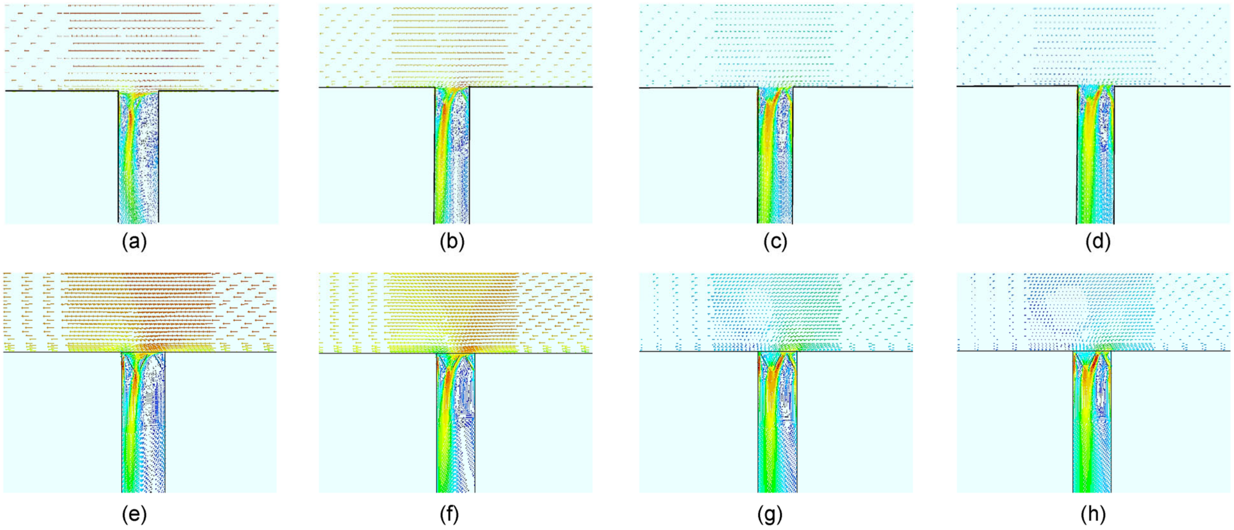

Fig. 4 Velocity vector distribution fields for different velocity ratios

(a) 3D method, v/V=0.2; (b) 3D method, v/V=0.3; (c) 3D method, v/V=1.0; (d) 3D method, v/V=1.5; (e) 2D method, v/V=0.2; (f) 2D method, v/V=0.3; (g) 2D method, v/V=1.0; (h) 2D method, v/V=1.5

Table 2 Local resistance coefficients under different opening angles and velocity ratios

v/V	Resistance coefficient ξ									
	θ=90°	θ=78.75°	θ=67.5°	θ=56.25°	θ=50.625°	θ=45°	θ=39.375°	θ=33.75°	θ=28.125°	θ=22.5°
16.7	0.741	1.10	2.00	6.09	10.7	19.4	36.7	73.0	156	403
10.0	0.757	1.12	1.94	6.10	10.7	19.4	36.7	73.0	156	403
5.0	0.842	1.19	2.07	6.17	10.7	19.5	36.8	73.2	157	403
2.5	1.07	1.44	2.30	6.43	10.9	19.6	37.1	73.6	157	403
1.3	1.79	2.11	2.12	7.29	12.0	20.7	38.3	75.0	159	408
0.6	4.01	4.25	4.72	10.7	15.9	25.3	42.9	80.2	164	419
0.5	5.70	5.63	6.16	12.0	17.3	26.5	46.1	82.7	168	421
0.4	8.12	7.86	8.01	13.7	19.0	27.9	45.8	82.9	171	424
0.3	11.1	10.4	11.1	15.5	21.0	30.2	47.4	84.8	170	429
0.2	27.8	28.4	29.8	32.1	34.2	44.8	62.5	97.6	182	492
0.1	106	105	105	108	109	112	126	161.9	250	574

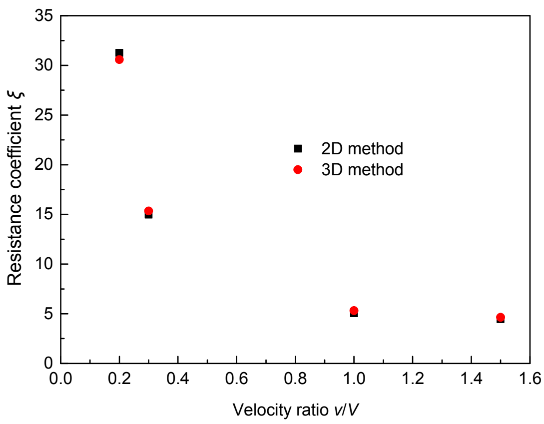

Fig. 5 Comparison of local resistance coefficients obtained from 3D and 2D methods

2. When the velocity ratio v/V is constant, ξ tends to increase as the opening angle θ decreases. This is especially obvious when θ is small.

3. When v/V>2.5, ξ under each opening angle situation tends to be a constant value, which reveals that ξ is related only to the opening angle θ when v/V>2.5.

4. When v/V is close to 0.1, curves for ξ corresponding to opening angles <45° approach each other.

Based on the analysis above, curves for ξ under the conditions θ≥45° and θ<45° were plotted, respectively (Figs. 6a and 6b).

According to Fig. 6, when v/V<2.5, the resistance coefficient curves respond differently under the conditions of large or small opening angles as the velocity ratio decreases:

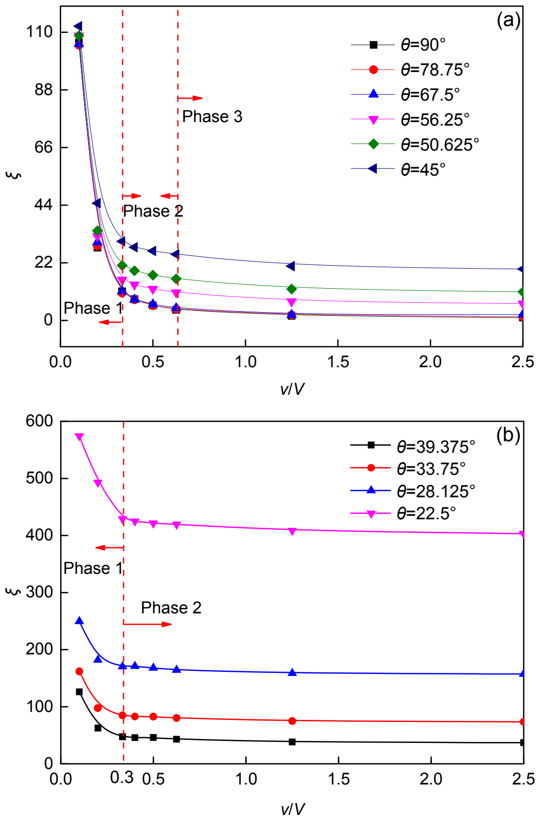

Fig. 6 Local resistance coefficient curves for v/V ratios <2.5

(a) Curves for large opening angles; (b) Curves for small opening angles

1. The growth pattern of curves for large opening angles ($\theta \geq 45°$) can be divided into three phases: a slow growth phase (phase 3, $0.6 \leq v/V < 2.5$), a quicker growth phase (phase 2, $0.3 \leq v/V < 0.6$), and the quickest growth phase (phase 1, $0 < v/V < 0.3$). In the quickest growth phase, the curves gradually approach each other and confluence is achieved when v/V is close to 0.1. We conclude that when v/V is quite small, i.e. close to 0.1, ξ is related only to the velocity ratio v/V.

2. The growth pattern of curves of small opening angles ($\theta < 45°$) can be divided into two phases: a slow growth phase (phase 2, $0.3 \leq v/V < 2.5$) and a quick growth phase (phase 1, $0 < v/V < 0.3$).

The above conclusions can be explained as follows: Changes in flow direction and section contraction and expansion are the main causes of pressure loss for air flow through the damper (Oliveira and Pinho, 1997; Kalpakli and Örlü, 2013). The pressure loss caused by a change in flow direction is closely related to the flow rate in the duct, while the loss caused by section change depends only on the flow rate through the damper and the opening angle. Thus, when the velocity ratio v/V is quite large, the pressure loss depends mainly on the section change; as the flow rate increases within the duct, pressure loss caused by the change in flow direction starts accounting for more of the total pressure loss and eventually becomes the dominant factor.

3 Design strategy for uniform air flow distribution

3.1 Static pressure distribution in the duct

In a tunnel transverse ventilation system, there is an air supply duct with numerous dampers and a closed end. A fixed amount of fresh air flows into the duct from the entrance and flows uniformly out of the duct through the dampers. The dampers are numbered from the end of the duct. The air supply system is illustrated in Fig. 7.

Since the amount of air flowing out from each damper is the same, the air flow velocity in the air supply duct decreases linearly, and its distribution in the air duct can be expressed as

$$V_x = \frac{x}{L} \cdot V_N, \tag{4}$$

where L represents the length of the duct, V_N is the air flow velocity at the entrance, V_x is the velocity at a position that is x meters away from the end of the duct, and the subscripts refer to the positions related to the values.

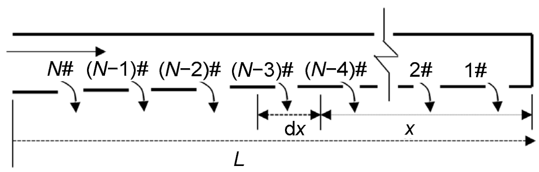

Fig. 7 Schematic diagram of an air supply system in a tunnel transverse ventilation system

Selecting the damper that is x meters away from the end of the duct as an analysis object, two sections with an interval of dx are located in the upstream and downstream directions of the damper, respectively. A Bernoulli equation can be established between these two sections:

$$P_x+\frac{\rho V_x^2}{2}+\frac{\lambda}{d}\cdot\frac{\rho V_x^2}{2}\mathrm{d}x+\alpha\frac{\rho V_x^2}{2}=P_x+\mathrm{d}P_x+\frac{\rho\left(V_x+\mathrm{d}V_x\right)^2}{2},\tag{5}$$

where P_x represents the static pressure of the section in the upstream direction, dP_x and dV_x are the variations in static pressure and velocity between the two selected sections respectively, d is the hydraulic diameter of the duct section, λ is a frictional factor, and α is the local resistance coefficient along the duct air flow direction caused by the damper.

Combining Eqs. (4) and (5), the static pressure variation dP_x can be expressed as

$$\mathrm{d}P_x=\frac{\lambda}{d}\cdot\frac{\rho V_N^2}{2}\cdot\frac{x^2}{L^2}\mathrm{d}x-\rho V_x\mathrm{d}V_x+\alpha\frac{\rho V_x^2}{2}.\tag{6}$$

Integrating both sides of the formula from a range of zero to x, we can obtain a formula to calculate the static pressure difference between the selected section and the closed end of the duct:

$$P_x-P_0=\left(\frac{\lambda x}{3d}-1\right)\frac{\rho V_x^2}{2}+\int_0^x\alpha\frac{\rho V_x^2}{2}.\tag{7}$$

When the ratio of the outflow from the damper to the flow inside the duct is less than 0.2, which is quite common in an air supply duct, α is only from 0.02 to 0.03 (Rong et al., 2010). So, the last term of Eq. (7) is usually negligible. Thus, Eq. (7) can be amended as

$$P_x=P_0+\left(\frac{\lambda x}{3d}-1\right)\frac{\rho V_x^2}{2}.\tag{8}$$

Eq. (8) shows that the minimum static pressure within the air duct is not located at the end of the air duct. According to energy conservation, part of the dynamic pressure loss is converted into a static pressure increment, while the loss caused by the local and frictional resistances transforms to other forms of energy. As a result, there is a balance point between these two kinds of energy conversion, and the specific location of the minimum static pressure is related to the frictional factor λ and hydraulic diameter d.

3.2 Strategy for opening angle regulation

Assuming that the interval between two dampers is l, and the first damper is half the distance away from the closed end of the duct, then the distance x_n between the closed end of the duct and the damper numbered n can be expressed as

$$x_n=\frac{nL}{N}-\frac{l}{2},\tag{9}$$

where N represents the total number of dampers. Combining Eqs. (8) and (9) provides a formula to calculate the static pressure at each damper position:

$$P_n=P_0+\left[\frac{\lambda}{3d}\left(\frac{nL}{N}-\frac{l}{2}\right)-1\right]\cdot\frac{\rho}{2}\left(\frac{nV_N}{N}\right)^2.\tag{10}$$

Taking Eq. (10) back to Eq. (1) and replacing P_r with P_n, the relationship between the static pressure inside and outside the duct is given by

$$P_n+\frac{\rho}{2}\left(\frac{nV_N}{N}\right)^2=P_\mathrm{e}+\xi_n\frac{\rho}{2}v^2+\frac{\rho}{2}v^2.\tag{11}$$

In a tunnel transverse system, P_e refers to the static pressure in the tunnel at the damper position, and is related to traffic, meteorological parameters, and the structure of the tunnel. To precisely determine P_e is complex, but it is usually quite small when compared with the static pressure inside the duct. Thus, in a primary design stage, P_e is always taken as zero, i.e. the same to the barometric pressure. Based on this concept, a formula to calculate the local resistance coefficient ξ_n can be obtained as

$$\left(\xi_n+1\right)\frac{\rho}{2}v^2=P_0+\frac{\lambda}{3d}\left(\frac{nL}{N}-\frac{l}{2}\right)\frac{\rho}{2}\cdot\left(\frac{n}{N}\cdot V_N\right)^2.\tag{12}$$

According to Eq. (12), to calculate the local resistance coefficient, the static pressure P_0 at the end of the duct must be determined first. Two points need to be considered in determining P_0.

1. Meeting the minimum pressure difference requirement

As revealed by Eq. (8), there is a minimum static pressure position within the duct that leads to the smallest pressure difference between the two sides of a damper. The number of the damper located at the minimum pressure position, $n_{\min}$, can be determined as

$$n_{\min}=\left(\frac{3d}{\lambda}+\frac{l}{2}\right)\frac{L}{N}. \tag{13}$$

The static pressure at that damper position is

$$P_{n,\min}=\left[\frac{\lambda}{3d}\left(\frac{n_{\min}L}{N}-\frac{l}{2}\right)-1\right]\cdot\frac{\rho}{2}\left(\frac{n_{\min}V_N}{N}\right)^2. \tag{14}$$

To effectively implement air supply, $P_{n,\min}$ should be large enough to overcome the flow resistance caused by the damper. This can be expressed as

$$\frac{2\left(P_{n,\min}-P_{\mathrm{e}}\right)+\rho\left(V_{x,\min}^2-v^2\right)}{\rho v^2}\geq\xi_{\min}. \tag{15}$$

The local resistance coefficient $\xi_{\min}$ can be determined in advance according to the largest opening angle and the velocity ratio in the primary design stage.

2. Convenient adjustment of the opening angle

In a tunnel transverse ventilation system, the velocity ratios at the entrance region of the duct are usually small (close to 0.1). In this circumstance, a small static pressure difference between the two sides of the damper will lead to a large opening angle (θ≥45°) design, according to Table 2 and Fig. 6. However, curves for large opening angles are too close to allow selection of the right opening angle for design. Eq. (8) reveals that the pressure difference between two sections in the duct depends only on the entrance velocity. So, in the design of uniform air flow distribution, the pressure at the closed end should be large enough to ensure that the entrance-region opening angle design complies the small opening angle curves.

The analysis above provides a clear design strategy for uniform air flow distribution in tunnel transverse systems, which can be reduced by: (1) Designing the basic parameters for the air supply duct (including the interval of the dampers) and determining the velocity ratios for dampers at each location; (2) Calculating the static pressure distribution along the duct; (3) Ascertaining the position and the corresponding damper where the minimum static pressure is located, and assigning the opening angle for the damper; (4) Selecting an appropriate static pressure for the end of the duct, and calculating the local resistance coefficient at each damper position; (5) Combining the calculated results with Table 2 and Figs. 6 and 7 to determine the opening angle for each damper through a method of interpolation.

4 Design case

To verify the reliability of the opening angle design strategy, a 600-m air supply duct was taken as a design case. Dampers with a length of 0.6 m and width of 1 m were installed on the duct, and the interval was set as 20 m. The hydraulic diameter of the duct is 4 m, the air density is 1.225 kg/m^3, and the frictional factor is 0.042. Assigning the fresh air requirement per unit length of tunnel as 0.024 m^3/s, the entrance velocity is 7.2 m/s. After many trial calculations, both the minimum pressure difference requirement and the convenience of the opening angle adjustment were satisfied when taking 10 Pa as the duct end static pressure. In this design case, every three consecutive dampers were designed to have the same opening angle.

With the information given above, the static pressures at each damper position were first calculated, and then with a combination of velocity ratios, local resistance coefficients were obtained. Opening angles (Table 3) were finally designed by means of interpolation.

To verify the calculation results, a CFD method was also carried out. With the designed opening angles, a 2D model was built, as presented in Fig. 8. In this model, boundary layer grids with a thickness of 0.004 m were appended to both edges of the duct, and denser grids were applied in regions (±0.25 m) around each damper. With trial simulations, the roughness height and roughness constant were set as 0.026 m and 0.8, respectively, as these values led to a satisfactory consistency with the assigned frictional factor. Numerical and theoretical results for static pressure and velocity distributions were compared (Figs. 9 and 10). To quantitatively analyze the accuracy of the design results, the root mean square error (RMSE) was calculated. The RMSE is the square root of the average of squared errors, and is sensitive to differences between two samples of data, especially when outliers exist. In general, a lower RMSE is better than a higher one, and a value of 0 (never achieved in practice) would indicate a perfect fit to the data. The RMSE was calculated as

$$\mathrm{RMSE}=\sqrt{\frac{\sum_{i}^{m} d_i^2}{m}}, \tag{16}$$

where m is the number of data in each sample and d_i represents the difference between a predicted value and an observed value.

The calculated RMSE values were 1.12 Pa for static pressures and 0.0083 m/s for velocities at each damper position. In view of the scale of the numbers analyzed, both these errors are acceptable.

Table 3 Opening angle design list

No.	Distance to the duct end (m)	Velocity (m/s)	Static pressure (Pa)	Local resistance coefficient ξ_i	Velocity ratio v/V_n	Opening angle θ (°)	Applied dampers
2#	30	0.48	9.87	24.69	1.67	43.09	1#–3#
5#	90	1.20	9.40	25.51	0.67	44.55	4#–6#
8#	150	1.92	8.93	27.87	0.42	44.78	7#–9#
11#	210	2.64	8.87	32.77	0.30	44.44	10#–12#
14#	270	3.36	9.62	41.25	0.24	43.54	13#–15#
17#	330	4.08	11.58	54.32	0.20	41.85	16#–18#
20#	390	4.80	15.15	73.00	0.17	39.15	19#–21#
23#	450	5.52	20.73	98.32	0.14	36.23	22#–24#
26#	510	6.24	28.72	131.29	0.13	33.86	25#–27#
29#	570	6.96	39.52	172.94	0.11	31.50	28#–30#

(a) (b)

Fig. 8 Model for the design case
(a) Model for the whole duct; (b) Local mesh refinement

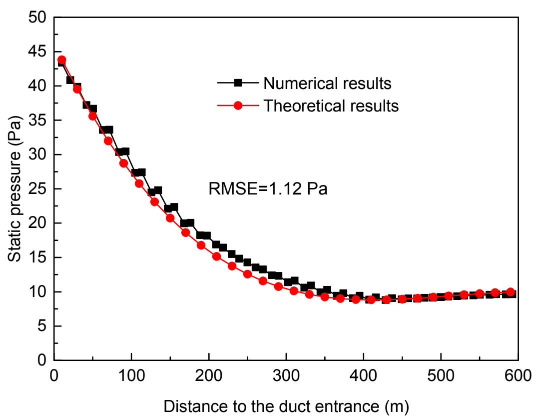

Fig. 9 Comparison of static pressure distribution

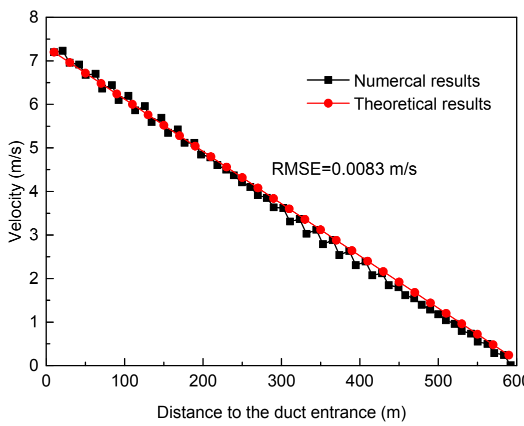

Fig. 10 Comparison of velocity distribution

5 Conclusions

A uniform air flow distribution is especially needed to dilute vehicle exhaust gases or emissions to acceptable concentrations in tunnel transverse ventilation systems. However, few investigations have focused on this field. Multi-blade diverter dampers are engineered specifically for gas exhaust applications and can be directly installed on an air supply duct. Air flow volume adjustment can be adjusted conveniently and flexibly with the damper just by setting different blade opening angles. This study focused mainly on the uniform air flow distribution design of a multi-perforated air supply duct with a damper. The aim was to achieve a uniform outflow distribution at each damper position along the duct.

Both 2D and 3D CFD simulation methods were carried out to investigate how the ratio of the velocity in the duct to that flows through the damper, and the blade opening angle affect the local resistance coefficient ξ arising when air flows out of the duct through the damper. Simulation results revealed that: when $v/V>2.5$, ξ is related only to the opening angle θ; when $v/V\leq 2.5$, ξ caused by large opening angles ($\theta\geq 45°$) and small opening angles ($\theta<45°$) show different growth patterns as the velocity ratio decreases; when v/V is close to 0.1, ξ caused by large opening angles is related only to the velocity ratio v/V.

With the simulation results, theoretical analysis based on the Bernoulli equation was implemented to establish the relationship between the local resistance coefficient and the opening angle. Finally, a uniform air flow distribution design strategy corresponding to the opening angle adjustment was obtained. In addition, a sufficient consistency between the theoretical and numerical calculation results in a design case verified the reliability of the strategy.

This investigation is helpful in the preliminary design of tunnel transverse ventilation systems and similar projects. However, more work is still needed to provide a comprehensive design strategy.

References

Ascough GW, Kiker GA, 2002. The effect of irrigation uniformity on irrigation water requirements. *Water SA*, 28(2):235-242. https://doi.org/10.4314/wsa.v28i2.4890

Chen A, Sparrow EM, 2009a. Effect of exit-port geometry on the performance of a flow distribution manifold. *Applied Thermal Engineering*, 29(13):2689-2692. https://doi.org/10.1016/j.applthermaleng.2008.12.035

Chen A, Sparrow EM, 2009b. Turbulence modeling for flow in a distribution manifold. *International Journal of Heat and Mass Transfer*, 52(5-6):1573-1581. https://doi.org/10.1016/j.ijheatmasstransfer.2008.08.006

El Moueddeb K, Barrington S, Barthakur N, 1997. Perforated ventilation ducts: part 1, a model for air flow distribution. *Journal of Agricultural Engineering Research*, 68(1): 21-27. https://doi.org/10.1006/jaer.1997.0176

Farajpourlar M, 2017. On the prediction of uniformity of air flow out from manifold distribution. *Materialwissenschaft und Werkstofftechnik*, 48(3-4):249-254. https://doi.org/10.1002/mawe.201600765

Foust J, Rockwell D, 2007. Flow structure associated with multiple jets from a generic catheter tip. *Experiments in Fluids*, 42(4):513-530. https://doi.org/10.1007/s00348-006-0249-z

Ibukiyama S, 1957. The calculation methods of static pressures in the ventilation ducts of uniform area with slots of equal size at equal intervals and opening areas of those slots. *Transactions of the Japan Society of Civil Engineers*, 47:30-37. https://doi.org/10.2208/jscej1949.1957.47_30

Ji CZ, Zhang X, Jiang M, et al., 2010. Numerical simulation of influence of 90°-bend pipeline geometric shape on local loss coefficient. International Conference on Mechanical and Electrical Technology, p.668-672. https://doi.org/10.1109/ICMET.2010.5598446

Jo HJ, Chun KM, Min DK, et al., 2017. A study on the program development for optimizing the supply and exhaust port opening ratio in road tunnels with transverse ventilation system. *Journal of Korean Tunnelling and Underground Space Association*, 19(3):517-532. https://doi.org/10.9711/KTAJ.2017.19.3.517

Kalpakli A, Örlü R, 2013. Turbulent pipe flow downstream a 90° pipe bend with and without superimposed swirl. *International Journal of Heat and Fluid Flow*, 41:103-111. https://doi.org/10.1016/j.ijheatfluidflow.2013.01.003

Kareeri AA, Zughbi HD, Al-Ali HH, 2006. Simulation of flow distribution in radial flow reactors. *Industrial & Engineering Chemistry Research*, 45(8):2862-2874. https://doi.org/10.1021/ie050027x

Kim S, Choi E, Cho YI, 1995. The effect of header shapes on the flow distribution in a manifold for electronic packaging applications. *International Communications in Heat and Mass Transfer*, 22(3):329-341. https://doi.org/10.1016/0735-1933(95)00024-S

Lee S, Moon N, Lee J, 2012. A study on the exit flow characteristics determined by the orifice configuration of multi-perforated tubes. *Journal of Mechanical Science and*

Technology, 26(9):2751-2758.
https://doi.org/10.1007/s12206-012-0721-z

Lesser N, Horowitz F, King K, 1987. Transverse ventilation system of the Holland tunnel evaluated and operated in semi-transverse mode. *Transportation Research Record*, 1150:24-28.

Li JSM, Chow WK, 2003. Numerical studies on performance evaluation of tunnel ventilation safety systems. *Tunnelling and Underground Space Technology*, 18(5):435-452.
https://doi.org/10.1016/S0886-7798(03)00023-3

Oliveira PJ, Pinho FT, 1997. Pressure drop coefficient of laminar Newtonian flow in axisymmetric sudden expansions. *International Journal of Heat and Fluid Flow*, 18(5):518-529.
https://doi.org/10.1016/S0142-727X(97)80010-0

Rong GW, Wei WL, Liu YL, 2010. 3D numerical simulation for hydraulic characteristics of turbulent flow in bifurcated duct. *Journal of Hydraulic Engineering*, 41(4): 398-405 (in Chinese).
https://doi.org/10.13243/j.cnki.slxb.2010.04.011

Singh RK, Rao AR, 2009. Simplified theory for flow pattern prediction in perforated tubes. *Nuclear Engineering and Design*, 239(10):1725-1732.
https://doi.org/10.1016/j.nucengdes.2009.05.028

VanGilder JW, Schmidt RR, 2005. Airflow uniformity through perforated tiles in a raised-floor data center. AMSE Pacific Rim Technical Conference and Exhibition on Integration and Packaging of MEMS, NEMS, and Electronic Systems Collocated with the ASME, p.493-501.
https://doi.org/10.1115/IPACK2005-73375

Wang J, Priestman GH, Wu D, 2001. A theoretical model of uniform flow distribution for the admission of high-energy fluids to a surface steam condenser. *Journal of Engineering for Gas Turbines and Power*, 123(2): 472-475.
https://doi.org/10.1115/1.1359237

Ye WB, 2017. Design method and modeling verification for the uniform air flow distribution in the duct ventilation. *Applied Thermal Engineering*, 110:573-583.
https://doi.org/10.1016/j.applthermaleng.2016.08.177

Yu HQ, 2013. Engineering Fluid Mechanics (3rd Edition). Southwest Jiaotong University Press, Chengdu, China, p.122-128 (in Chinese).

中文概要

题　目：隧道横向式通风系统中的等量送风设计方法研究

目　的： 公路隧道在采用横向式通风系统时，送风道内的空气应通过送风孔均匀地输送至隧道内，以满足整个隧道范围内的新鲜空气补充和污染物稀释的需求。但是，目前的隧道通风设计规范并没有明确的等量送风设计方法，且业界关于该问题的研究也极为缺乏。考虑到多页对开式风阀在风量调整方面的便利性与实用性，本文旨在通过明确风阀风阻特性以及等量送风管道内外静压的分布规律，研究一种通过调整风阀开角来实现风孔风量控制的理论设计方法。

创新点： 1. 结合量纲分析与数值模拟分析方法得出多页对开式风阀的风阻特性；2. 通过对等量送风道内外部建立一元伯努利方程，得出等量送风管道内的静压分布规律；3. 结合风阀风阻特性以及管道内外静压分布规律，得出一种基于压力平衡的风阀叶片开角理论调节方法，且该方法可以实现各风孔送风风量的理论控制。

方　法： 1. 利用量纲分析方法得出多页对开式风阀风阻特性的影响因素；2. 利用二维和三维数值分析方法计算得出不同叶片开角和风速比值条件下的风阀阻力系数（表 2 和图 6）；3. 通过理论分析，在送风道内部和风阀内外侧断面间建立一元伯努利方程，得到风道内的风速与静压分布规律，以及通过调节开角实现风量控制的理论设计方法；4. 利用数值分析方法对研究得到的等量送风理论设计方法进行可行性验证（图 9 和 10）。

结　论： 1. 影响多页对开式风阀风阻特性的 2 个因素分别是风阀的叶片开角和风道与风阀内的风速比值；2. 结合等量送风管道内静压分布规律以及风阀风阻特性，可以通过调整叶片开角实现风阀送风风量的理论控制；3. 数值验证结果表明，通过控制叶片开角来实现风阀出风风量的理论控制方法具备可行性且精度较高。

关键词： 多孔送风管；计算流体力学；局部阻力；等量送风；横向通风